Applied Physics Letters

RESEARCH ARTICLE | MAY 23 2024

Ultrafast nanometric resolution spatiotemporal measurement of ambipolar diffusivity and carrier-phonon coupling in doped and undoped silicon FREE

Mauricio Segovia ; Xianfan Xu

Appl. Phys. Lett. 124, 212104 (2024)
https://doi.org/10.1063/5.0205647

AIP Publishing

Applied Physics Letters ARTICLE pubs.aip.org/aip/apl

Ultrafast nanometric resolution spatiotemporal measurement of ambipolar diffusivity and carrier-phonon coupling in doped and undoped silicon

Cite as: Appl. Phys. Lett. **124**, 212104 (2024); doi: 10.1063/5.0205647
Submitted: 27 February 2024 · Accepted: 15 May 2024 ·
Published Online: 23 May 2024

Mauricio Segovia and Xianfan Xu[a)]

AFFILIATIONS

School of Mechanical Engineering and Birck Nanotechnology Center, Purdue University, West Lafayette, Indiana 47907, USA

[a)]Author to whom correspondence should be addressed: xxu@ecn.purdue.edu

ABSTRACT

Understanding and determination of the ambipolar diffusivity of a semiconductor is fundamental for predicting device behavior and optimizing its performance. Ultrafast pump-probe measurements allow for the determination of energy carrier dynamics with sub-picosecond resolution. Due to the inherent diffusive nature of carriers, measurements with a high spatial resolution are needed, in addition to the traditional pump-probe system, to determine not only the carrier dynamics but also the spatial extent caused by carrier diffusion as well. In this work, a spatiotemporal measurement system with ultrafast temporal and nanometric spatial resolution, together with a comprehensive transport model, is used to determine the ambipolar diffusivity and carrier-phonon energy coupling time in both undoped and doped silicon. The results show that as the carrier density increases, the measured ambipolar diffusivity decreases with minimal variation in the carrier-phonon energy coupling time. In general, this work demonstrates an optical-based method for determining ambipolar diffusivity in a semiconductor material.

During optical excitation of a semiconductor by an ultrafast laser, excited carriers undergo changes in their Fermi–Dirac distributions and are thrown into a non-equilibrated state.[1] After momentum randomization, the energy of carriers relaxes via a variety of mechanisms from carrier-carrier scattering to carrier-optical phonon scattering and others. During these relaxation processes, diffusion of excited carriers occurs as well as energy exchange with the underlying phonon system of the semiconductor. These picosecond timescale processes require fast measurement techniques. Ultrafast spectroscopy is a powerful tool that allows one to measure the optical response of a semiconductor, resulting in a temporal trace of an observable that can be related to the underlying transport properties. Since diffusion is inherently a spatial process, the traditional ultrafast pump-probe system is modified in this work to include a spatial scanning pump with nanometric spatial resolution. This spatiotemporal measurement has been used to study the diffusion process of a plethora of materials. Metals have been studied to show the electronic contribution to the overall diffusion process during early delay times.[2–4] The ultrafast optical response of semiconductors was measured to study the overall response of excited carriers.[5–8] Moreover, some newly developed materials have also been studied to elucidate the relaxation dynamics after ultrafast excitation.[9–12] This work intends to use the high-resolution spatiotemporal pump-probe system to determine two important transport parameters that dictate energy relaxation in semiconductors: the ambipolar diffusivity and the carrier-phonon energy coupling time.

The spatiotemporal pump-probe measurement is used to study the ultrafast dynamics of undoped, n-type, and p-type ⟨100⟩ silicon with varying initial carrier densities. Briefly, an 80 MHz Ti:sapphire laser, centered at 800 nm (1.55 eV) with a compensated (CM) pulse width of 250 fs full width at half maximum (FWHM), is split into a pump and probe arm as seen in Fig. 1(a). The pump arm is then modulated by an electro-optical modulator (EOM) at 90 kHz and frequency doubled to 400 nm (3.10 eV) with the use of a barium borate (BBO) crystal. The probe arm is delayed with a mechanical delay stage (DS) and used for balance detection (BD). Both the pump and probe are focused to 500 nm FWHM, near diffraction limited beam waists, with a dry 0.90 NA objective (O). The pump and probe incident fluences are measured to be 2.0 and 0.1 mJ cm^{-2}, respectively. To maintain

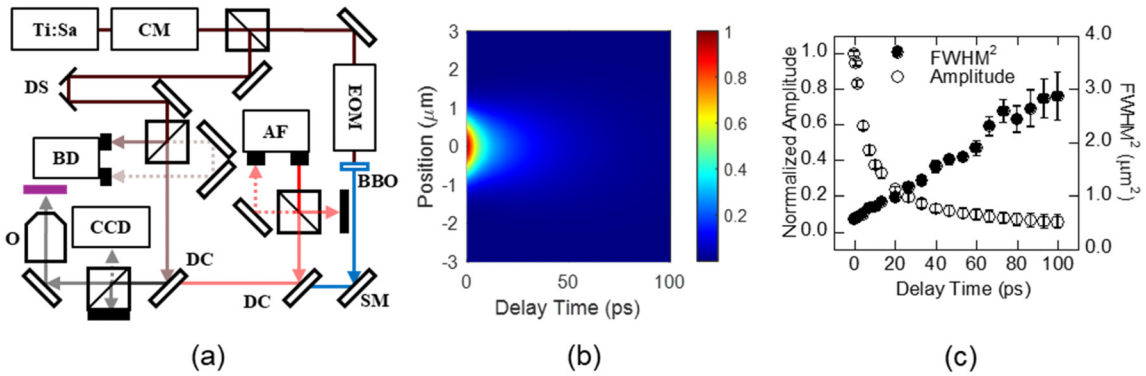

FIG. 1. (a) A schematic of the spatiotemporal pump-probe setup. Here, a sub-picosecond 3.1 eV pump and 1.55 eV probe are used to measure the spatial extent of the reflectance change on the sample. (b) A full colormap of the normalized measured reflectance profile as a function of the pump-probe displacement and temporal delay. (c) The normalized amplitude (open circles) and the spatial FWHM^2 (closed circles) of the reflectance profile are plotted as a function of temporal delay.

consistent beam waist sizes at the irradiated surface of interest, a continuous autofocusing system (AF) is used.[13] Additionally, an imaging system (CCD) is used to ensure the sample surface is free of superficial defects before the start of experimentation. All beams are combined to a single optical path with the aid of dichroic mirrors (DC). The temporal resolution of the system is dictated by the FWHM pulse width of both the pump and probe; here, the pulse widths are measured to be 500 fs via autocorrelation at the sample plane. The nanometric displacement of the pump relative to the probe has a step size of 2 nm at the sample plane, determined by precisely mapping the position of the pump beam waist via knife edge measurements as a function of the actuation of the piezo-actuated scanning tip/tilt mirror (SM). The uncertainty of a measured FWHM (by extension, the FWHM^2) is determined by the uncertainty in the displacement of the pump and the uncertainty in the probe detection system, which is dictated by the signal-to-noise of the balance detection system, via a Monte Carlo approach as follows: first, the temporal delay is fixed, and the pump is displaced relative to the probe, producing a spatial trace of the reflectance response. A FWHM value is determined by fitting a Gaussian curve to this trace. Next, the experimentally measured trace is modified, point by point, by sampling the probability distributions that closely describe the position and signal-to-noise ratio as random variables, effectively simulating a measured spatial trace. This process is repeated 10,000 times to produce a distribution of possible FWHM values. The uncertainty in a measured FWHM is then defined as plus or minus twice the standard deviation of this distribution. All experimental FWHM values are measured to within 10% uncertainty or less. Details of the experimental setup and the measurement uncertainty quantification can be found in earlier works.[3,8]

A piece of ⟨100⟩ undoped silicon with an initial carrier density of $10^{12}\,\mathrm{cm}^{-3}$ is first studied, and the spatiotemporal reflectance measurement is presented in Figs. 1(b) and 1(c). Due to the radially symmetric optical response of the sample, one-dimensional scan lines are performed as a function of temporal delay. Each scan line is fitted to a Gaussian curve to extract a peak signal value and a spatial FWHM. Hence, from a single experiment, the amplitude of the optical reflectance and its FWHM^2 are obtained. To extract the ambipolar diffusivity and carrier-phonon energy coupling time, a complete transport model containing the spatiotemporal evolution of carrier density [Fig. 2(a)], carrier temperature [Fig. 2(b)], and phonon temperature [Fig. 2(c)] is numerically solved. Details of this model can be found in previous works[8,14,15] and are summarized in supplementary material Note 1. The simulation results from the complete transport model are then given as inputs to an optical response model [Fig. 2(d)] at the probe photon energy to calculate the expected reflectance.[8,16–18] From the simulated reflectance, the difference with the experimentally measured normalized amplitude change and FWHM^2 datasets is computed as a function of the transport properties of interest. A standard least squares fitting routine is used, and the uncertainty in the reported value is calculated from a covariance/variance matrix method.[3] The best fitted results are shown in Figs. 2(e) and 2(f). Here, an ambipolar diffusivity value of $21 \pm 4\,\mathrm{cm}^2\,\mathrm{s}^{-1}$ and carrier-phonon energy coupling time of 4.5 ± 1.0 ps are determined for undoped silicon with uncertainty defined as plus or minus one standard deviation.

Here, it will be illustrated that a diffusion coefficient and a relaxation time can be deduced from a spatiotemporal measurement using a simplified model; the method of using the complete transport model to extract both ambipolar diffusivity and carrier–phonon coupling time is compared against this approach. First, it is noted that the governing PDEs are similar in functional form to a continuity equation with a time dependent diffusion coefficient, $D(t)$, and relaxation rate, Γ. Therefore, the spatiotemporal evolution of an observable in question, u, is expressed as

$$\frac{\partial u}{\partial t} + \nabla \cdot (-D(t)\nabla u) = -\Gamma u + S, \tag{1}$$

where S represents a Dirac delta source in time with a Gaussian spatial distribution, similar to the laser excitation source used in this work. The solution to Eq. (1) is given by

$$u(\vec{r}, t) = C\frac{e^{-\Gamma t}}{\sigma^3(t)}\exp\left(-4\log(2)\frac{|\vec{r}|^2}{\sigma^2(t)}\right), \tag{2}$$

$$\sigma^2(t) = \sigma_o^2 + 16\log(2)\int_0^t D(s)ds. \tag{3}$$

Here, $\vec{r}$ refers to a standard position vector, σ_o^2 is the initial spatial FWHM^2 of S taken as the beam waist of the focused pump laser, and C is a constant. From Eq. (2), the amplitude of the response, A, evolves

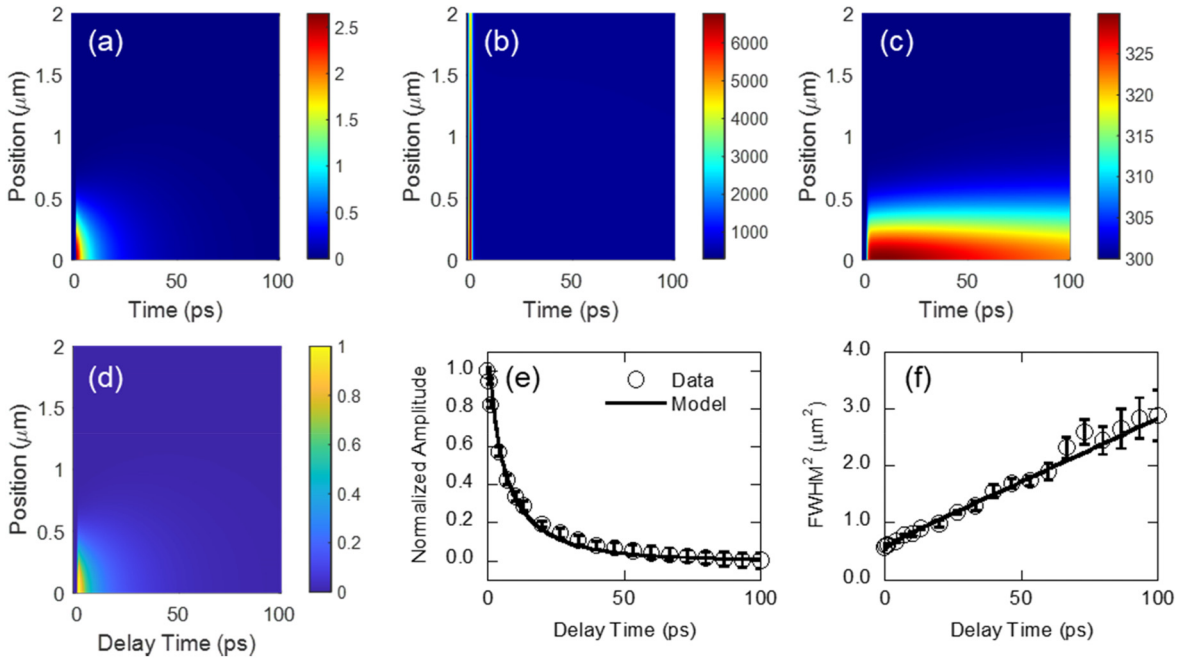

FIG. 2. A colormap of the simulated spatiotemporal evolution of the transport variables of interest: (a) carrier density (in units of 10^{26} m^{-3}), (b) carrier temperature (in units of K), and (c) phonon temperature (in units of K). Once all transport variables are simulated, the optical model is used to calculate the (d) expected normalized reflectance change at the probe wavelength. Here, both the (e) peak amplitude and the (f) FWHM^2 of the modeled reflectance map can be compared to the acquired data. The best fitted result from the complete transport model shows a good fit well within the experimental error.

as $e^{-\Gamma t}\sigma^{-3}(t)$, whereas the FWHM^2 of the observable evolves as $\sigma^2(t)$. A phenomenological expression[19] relating the derivative of the FWHM^2 to a diffusion coefficient is given as

$$\frac{\partial \sigma^2(t)}{\partial t} = 16\log(2) m D_m t^{m-1}, \tag{4}$$

where D_m is a generalized diffusion coefficient with appropriate units and m denotes the type of diffusion. Previous works have used this phenomenological expression to deduce a diffusion coefficient.[4,6,7,20] In this work, a normal diffusion process is first assumed, and the variable m is set to 1. A discussion of finding the values of m together with the generalized diffusion coefficient is given in the supplementary material Note 2. This simplified model shows that the FWHM^2 is insensitive to the relaxation rate of the observable and only to the generalized diffusion coefficient. As for the amplitude, the normalized sensitivities to the relaxation rate and FWHM^2 can be defined as $\delta\Gamma = \Gamma\,\partial A/\partial\Gamma$ and $\delta\sigma^2 = \sigma^2\,\partial A/\partial\sigma^2$, respectively. Defining a relaxation time as $\tau = \Gamma^{-1}$, the magnitude of the normalized sensitivity of the amplitude to the relaxation rate, relative to the FWHM^2, can be expressed as

$$|\delta\Gamma| = \frac{2}{3}\left(\frac{t}{\tau}\right)|\delta\sigma^2|. \tag{5}$$

Equation (5) states that if the relaxation time is small (equivalently, if the relaxation rate is large) relative to the time scales of interest, then the normalized sensitivity of the amplitude to Γ is larger in magnitude than the normalized sensitivity of the amplitude to $\sigma^2(t)$. Under these conditions, the experimental normalized amplitude dataset of the reflectance can be used to determine an underlying relaxation time (the reciprocal of the relaxation rate), and the experimental FWHM^2 dataset can be used to determine a diffusion coefficient.

We investigate the effects of density and type of dopants on the transport properties. Here, both n-type and p-type ⟨100⟩ silicon wafers are studied. The n-type silicon used in this work has an initial carrier density of 10^{14} cm^{-3} (low n) and 10^{19} cm^{-3} (high n); the p-type silicon has an initial carrier density of 10^{15} cm^{-3} (low p) and 10^{19} cm^{-3} (high p). Figures 3(a)–3(e) show the FWHM^2 for all five samples of silicon along with the best fitted complete transport model and Eq. (4) of the simplified model. It should be noted that due to the fast computational aspect of fitting the FWHM^2 dataset to Eq. (4), a complete 95% confidence band is constructed. The experimental FWHM^2 dataset is modified via a Monte Carlo approach to consider both the scattered aspects of the data itself and the experimental uncertainty in the FWHM^2. Over 10 000 simulated datasets are constructed, and a nonlinear fit to Eq. (4) is performed on each dataset. A distribution of all best fitted diffusion coefficients is obtained. The confidence interval is presented as upper and lower bounds (dashed lines in Fig. 3), and the uncertainty in the diffusion coefficient fitted to the simple model is defined as plus or minus twice the standard deviation. A summary of the best fitted ambipolar diffusion coefficient from the complete transport model and diffusion coefficient from the simple model is given in Fig. 3(f). Within the framework of the complete transport model, the mean value of the ambipolar diffusion coefficient is found to monotonically decrease as a function of the initial carrier density, irrespective of the dopant type. Using the framework of the simplified model, the fitted diffusion coefficient is found to have a similar trend with the

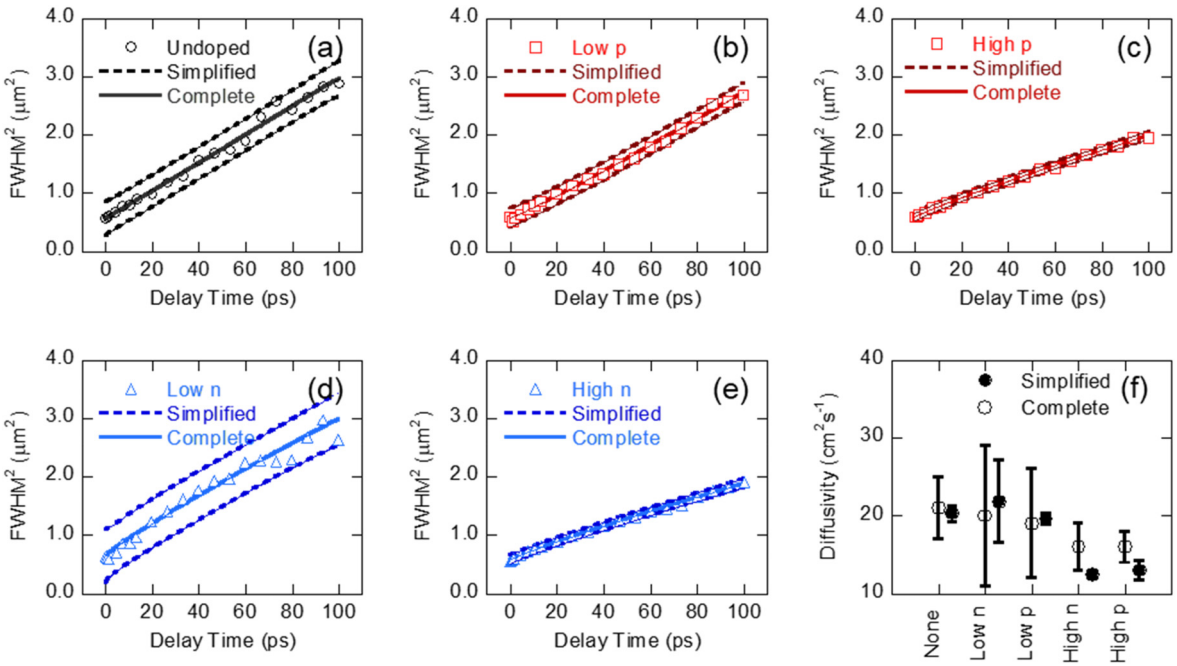

FIG. 3. Experimentally measured FWHM^2 plotted against the best fitted transport model result along with a 95% confidence interval calculated from the nonlinear curve fitting to Eq. (4) for (a) undoped, (b) lightly doped p-type, (c) heavily doped p-type, (d) lightly doped n-type, and (e) heavily doped n-type ⟨100⟩ silicon. (f) The ambipolar diffusion coefficient is found by fitting to the complete transport model (open circles) and from the nonlinear curve fit of the experimental data to exponential decay functions (closed circles).

diffusion coefficient decreasing as a function of the initial carrier density. Note that the uncertainty in the complete transport model is larger since two variables are determined simultaneously.

Figures 4(a)–4(e) show the normalized amplitude for all five samples of silicon plotted along with the best fitted complete transport model and the best nonlinear curve fitting result to multi-exponential functions. A summary of the best fitted carrier-phonon energy coupling time and relaxation time for all five samples is given in Fig. 4(f). Within the framework of the complete transport model, the carrier-phonon energy coupling time is found to have minimal variation with average values ranging from 3 to 5 ps. Figure 4(f) also shows that the relaxation time for these samples extracted using the simplified model is slightly different than those predicted by the complete transport model. The discrepancy may be because the simplified model does not consider the underlying coupled mechanisms such as diffusion of carrier and carrier-phonon energy relaxation. Therefore, the authors caution the sole use of the simplified model to extract the transport properties of interest. More discussions on the simplified model are given in the supplementary material Notes 2 and 3. Nevertheless, the use of simplified model is beneficial for an initial determination of possible transport properties and can be used as an initial guess when fitting the experimental datasets to the complete transport model, greatly reducing the computation cost of searching for the best fitted parameters. It is found that this methodology allowed the number of iterations of the fitting routine to decrease, reducing the total computational cost of extracting the two transport parameters in question using the complete transport model. Finally, it should be noted that the simplified model can hold physically meaningful results and can elucidate the diffusion process by allowing a rapid initial determination of both a relaxation time and a diffusion coefficient. Additional discussion on the time constants found by the fitting of multi-exponential functions can be found in the supplementary material Note 3.

Undoped ⟨100⟩ silicon has been shown to have a room temperature ambipolar diffusivity[20–22] between 18 and 36 $cm^2 s^{-1}$ along with carrier-phonon energy coupling time in the picosecond timescale.[17,23] The value of the ambipolar diffusivity determined from the ultrafast spatiotemporal measurement with the complete transport model is lower than the literature room temperature value. This observation is attributed to the large density change of carrier in the conduction band, which has been observed in previous measurements.[8,22,24] It is noted that the complete transport model used in this work assumes a generation of excess carriers with excess kinetic energy after crossing the bandgap (see the supplementary material Note 1). Therefore, the total number of photoexcited carriers is modeled as virtually independent of initial dopant type and initial density. With the absorbed pump fluence used in experimentation, a net maximum carrier density change of the excited carrier density ($\approx 10^{20}$ cm^{-3}) is simulated in all cases. Therefore, the results presented in this work are those of the total carrier density n, which is the sum of the initial carrier density, n_o, and the excited carrier density, Δn. Considering that the initial carrier density n_o for the undoped and lightly doped samples is several orders of magnitude less than that of the excited carrier density Δn, in these cases, their ambipolar diffusivities should be similar; this is consistent with the measurement results. On the other hand, in the highly doped cases, the initial carrier density n_o is within one order of magnitude of that of the excited

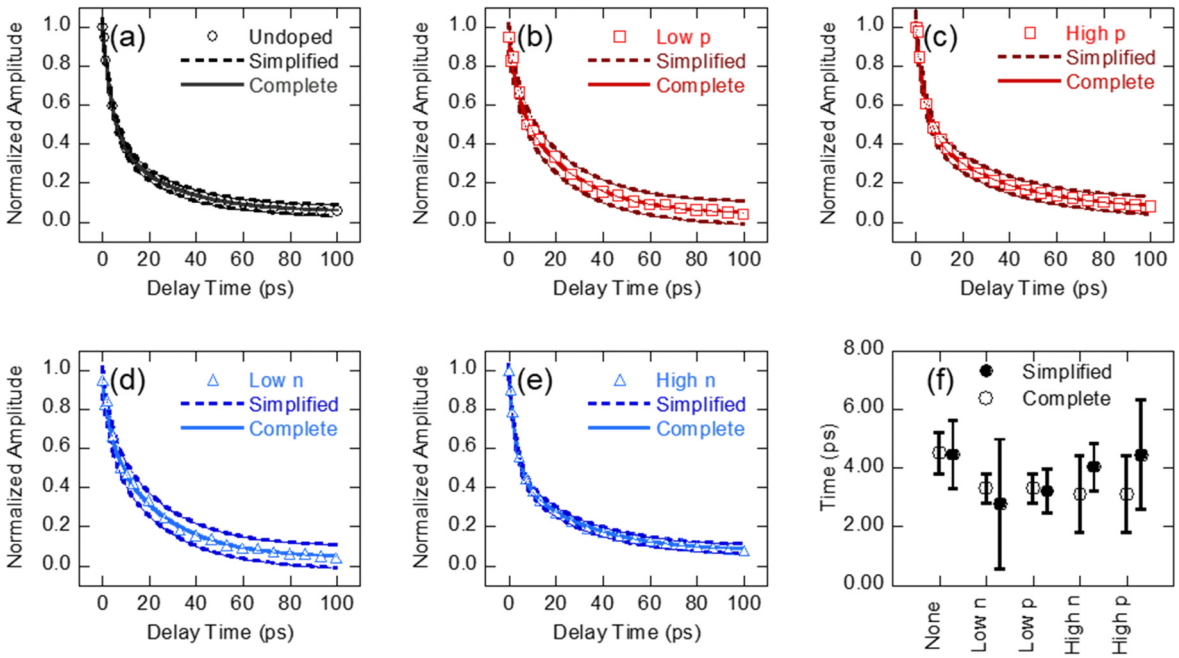

FIG. 4. Experimentally measured peak normalized amplitude plotted against the best fitted physical model result along with a 95% prediction band calculated from the nonlinear curve fitting to exponential curves for (a) undoped, (b) lightly doped p-type, (c) heavily doped p-type, (d) lightly doped n-type, and (e) heavily doped n-type ⟨100⟩ silicon. (f) The carrier-phonon energy coupling time is found from the complete transport model (open circles) and from the nonlinear curve fit of the experimental data to exponential decay functions (closed circles).

carrier density Δn, resulting in a higher total carrier density relative to the undoped and lightly doped cases. A decrease in the ambipolar diffusivity is observed, which is consistent with the trend that ambipolar diffusivity decreases with carrier density.[22]

In conclusion, an ultrafast spatiotemporal pump-probe system with sub-picosecond temporal resolution and nanometric spatial resolution was used to extract the ambipolar diffusivity and carrier-phonon energy coupling time of undoped, lightly doped, and heavily doped ⟨100⟩ silicon. A complete transport model accounting for changes in the excited carrier density, carrier energy, and phonon energy was used in combination with an optical transport model to determine two transport parameters: the carrier-phonon energy coupling time and the ambipolar diffusivity. It was found that the ambipolar diffusivity decreased as a function of carrier density, independent of dopant type. The carrier-phonon energy coupling time was also found to decrease with carrier density through the framework of the complete transport model; however, the experiment results have large uncertainties for determining the temperature dependency. The complete transport model was compared against a simpler model, which provides physically meaningful initial determination of possible transport properties. These possible transport values were then used as starting points when searching for the best fitted parameters with the complete transport model, reducing computational cost. The advantages of this experimental procedure allow one to simultaneously determine temporal and spatial transport properties of excited carriers in semiconductors with a single spatiotemporal measurement and can be expanded to the studies of other types of semiconductor materials including 2D semiconductor materials.

See the supplementary material for details of complete transport model, power law of the diffusion process, and discussion on time constants.

The financial support from the National Science Foundation (Grant No. CBET-2051525) is gratefully acknowledged.

AUTHOR DECLARATIONS

Conflict of Interest

The authors have no conflicts to disclose.

Author Contributions

Mauricio Segovia: Data curation (equal); Formal analysis (equal); Investigation (equal); Methodology (equal); Validation (equal); Visualization (equal); Writing – original draft (equal); Writing – review & editing (equal). **Xianfan Xu:** Conceptualization (equal); Investigation (equal); Project administration (equal); Supervision (equal); Writing – original draft (equal); Writing – review & editing (equal).

DATA AVAILABILITY

The data that support the findings of this study are available from the corresponding author upon reasonable request.

REFERENCES

[1]A. Othonos, "Probing ultrafast carrier and phonon dynamics in semiconductors," J. Appl. Phys. **83**(4), 1789 (1998).

[2]A. Block, M. Liebel, R. Yu, M. Spector, Y. Sivan, F. J. García De Abajo, and N. F. Van Hulst, "Tracking ultrafast hot-electron diffusion in space and time by ultrafast thermomodulation microscopy," Sci. Adv. **5**(5), eaav8965 (2019).
[3]M. Segovia and X. Xu, "High accuracy ultrafast spatiotemporal pump-probe measurement of electrical thermal transport in thin film gold," Nano Lett. **21**(17), 7228–7235 (2021).
[4]Y. K. Zhou, X. Z. Li, Q. N. Zhou, R. H. Xing, Y. Zhang, B. Bai, H. H. Fang, and H. B. Sun, "Transient superdiffusion of energetic carriers in transition metal dichalcogenides visualized by ultrafast pump-probe microscopy," Ultrafast Sci. **2022**, 0002.
[5]L. M. Smith, D. R. Wake, J. P. Wolfe, D. Levi, M. V. Klein, J. Klem, T. Henderson, and H. Morkoç, "Picosecond imaging of photoexcited carriers in quantum wells: Anomalous lateral confinement at high densities," Phys. Rev. B **38**(8), 5788–5791 (1988).
[6]B. A. Ruzicka, L. K. Werake, H. Samassekou, and H. Zhao, "Ambipolar diffusion of photoexcited carriers in bulk GaAs," Appl. Phys. Lett. **97**(26), 262119 (2010).
[7]E. E. M. Cating, C. W. Pinion, E. M. Van Goethem, M. M. Gabriel, J. F. Cahoon, and J. M. Papanikolas, "Imaging spatial variations in the dissipation and transport of thermal energy within individual silicon nanowires using ultrafast microscopy," Nano Lett. **16**(1), 434–439 (2016).
[8]M. Segovia and X. Xu, "Ultrafast, high resolution spatiotemporal mapping of energy transport dynamics for determination of energy transport properties in silicon," Phys. Rev. B **108**(12), 125202 (2023).
[9]N. Kumar, B. A. Ruzicka, N. P. Butch, P. Syers, K. Kirshenbaum, J. Paglione, and H. Zhao, "Spatially resolved femtosecond pump-probe study of topological insulator Bi_2 Se_3," Phys. Rev. B **83**(23), 235306 (2011).
[10]S. J. Yoon, Z. Guo, P. C. Dos Santos Claro, E. V. Shevchenko, and L. Huang, "Direct imaging of long-range exciton transport in quantum dot superlattices by ultrafast microscopy," ACS Nano **10**(7), 7208–7215 (2016).
[11]Z. Guo, Y. Wan, M. Yang, J. Snaider, K. Zhu, and L. Huang, "Long-range hot-carrier transport in hybrid perovskites visualized by ultrafast microscopy," Science **356**(6333), 59–62 (2017).
[12]S. Deng, E. Shi, L. Yuan, L. Jin, L. Dou, and L. Huang, "Long-range exciton transport and slow annihilation in two-dimensional hybrid perovskites," Nat. Commun. **11**(1), 1–8 (2020).
[13]Z. Bai and J. Wei, "Focusing error detection based on astigmatic method with a double cylindrical lens group," Opt. Laser Technol. **106**, 145–151 (2018).
[14]H. M. Van Driel, "Kinetics of high-density plasmas generated in Si by 1.06- and 0.53-μm picosecond laser pulses," Phys. Rev. B **35**(15), 8166 (1987).
[15]A. Rämer, O. Osmani, and B. Rethfeld, "Laser damage in silicon: Energy absorption, relaxation, and transport," J. Appl. Phys. **116**(5), 053508 (2014).
[16]K. Sokolowski-Tinten and D. von der Linde, "Generation of dense electron-hole plasmas in silicon," Phys. Rev. B **61**(4), 2643 (2000).
[17]A. J. Sabbah and D. M. Riffe, "Femtosecond pump-probe reflectivity study of silicon carrier dynamics," Phys. Rev. B **66**(16), 165217 (2002).
[18]E. Petrakakis, G. D. Tsibidis, and E. Stratakis, "Modelling of the ultrafast dynamics and surface plasmon properties of silicon upon irradiation with mid-IR femtosecond laser pulses," Phys. Rev. B **99**(19), 195201 (2019).
[19]V. Sposini, D. Krapf, E. Marinari, R. Sunyer, F. Ritort, F. Taheri, C. Selhuber-Unkel, R. Benelli, M. Weiss, R. Metzler, and G. Oshanin, "Towards a robust criterion of anomalous diffusion," Commun. Phys. **5**(1), 1–10 (2022).
[20]H. Zhao, "Temperature dependence of ambipolar diffusion in silicon on insulator," Appl. Phys. Lett. **92**(11), 112104 (2008).
[21]R. Brunetti, C. Jacoboni, F. Nava, L. Reggiani, G. Bosman, and R. J. J. Zijlstra, "Diffusion coefficient of electrons in silicon," J. Appl. Phys. **52**(11), 6713–6722 (1981).
[22]M. Rosling, H. Bleichner, P. Jonsson, and E. Nordlander, "The ambipolar diffusion coefficient in silicon: Dependence on excess-carrier concentration and temperature," J. Appl. Phys. **76**(5), 2855 (1994).
[23]B. Liao, B. Qiu, J. Zhou, S. Huberman, K. Esfarjani, and G. Chen, "Significant reduction of lattice thermal conductivity by the electron-phonon interaction in silicon with high carrier concentrations: A first-principles study," Phys. Rev. Lett. **114**(11), 115901 (2015).
[24]J. P. Callan, A. M. T. Kim, L. Huang, and E. Mazur, "Ultrafast electron and lattice dynamics in semiconductors at high excited carrier densities," Chem. Phys. **251**(1–3), 167–179 (2000).